Separation and Purification Technology 312 (2023) 123346

Contents lists available at ScienceDirect

Separation and Purification Technology

journal homepage: www.elsevier.com/locate/seppur

Incorporation of a pyrrolidinium-based ionic liquid/MIL-101(Cr) composite into Pebax sets a new benchmark for CO_2/N_2 selectivity

Nitasha Habib [a,b], Özce Durak [a,b], Alper Uzun [a,b,c,*], Seda Keskin [a,b,*]

[a] Department of Chemical and Biological Engineering, Koç University, Rumelifeneri Yolu, 34450 Sariyer, Istanbul, Turkey
[b] Koç University TÜPRAS Energy Center (KUTEM), Koç University, Rumelifeneri Yolu, 34450 Sariyer, Istanbul, Turkey
[c] Koç University Surface Science and Technology Center (KUYTAM), Koç University, Rumelifeneri Yolu, 34450 Sariyer, Istanbul, Turkey

ARTICLE INFO

Keywords:
Mixed matrix membrane (MMM)
Metal organic framework (MOF)
Ionic liquid (IL)
IL/MOF composite
CO_2 separation

ABSTRACT

Mixed matrix membranes (MMMs) offer a broad potential for energy efficient removal of CO_2 from flue gas and natural gas. In this study, we synthesized a novel ionic liquid (IL)/metal organic framework (MOF) composite, [MPPyr][DCA]/MIL-101(Cr), where [MPPyr][DCA] is 1-methyl-1-propyl pyrrolidinium dicyanamide, and incorporated it as a filler into Pebax to fabricate IL/MOF/polymer MMMs. The superior solubility of CO_2 in the [MPPyr][DCA] and the strong interactions between IL and CO_2 molecules boost the CO_2 selectivity of the membrane over N_2 and CH_4. The results showed that CO_2 permeability of the MMM having 15 wt.% [MPPyr][DCA]/MIL-101(Cr) composite as the filler (148 Barrer) was similar to that of pure Pebax membrane (134 Barrer), while the ideal CO_2/N_2 selectivity (1347) and ideal CO_2/CH_4 selectivity (122) of the MMM were 45- and 10-times higher compared to the selectivities of pure Pebax membrane, respectively. To the best of our knowledge, the remarkable enhancement in the CO_2/N_2 selectivity of the MMM sets a new benchmark value for the IL/MOF/polymer MMMs in the literature. These results demonstrate the great potential of using [MPPyr][DCA]/MIL-101(Cr) composite as a filler for the fabrication of highly selective IL/MOF/polymer MMMs for CO_2/N_2 and CO_2/CH_4 separations.

1. Introduction

Membrane-based CO_2 separation has been proven to be promising owing to its high efficiency, design simplicity, ease of fabrication, low energy requirement, and small carbon footprint [1,2]. Although polymer membranes have been widely used for gas separation, their separation performance is limited by the trade-off between permeability and selectivity, as shown with the Robeson's upper bound [3]. To overcome this limitation, mixed matrix membranes (MMMs), which are fabricated by dispersing porous fillers (zeolites, graphene oxide, carbon nanotubes, metal oxides, and metal organic frameworks (MOFs)) into the polymer matrix, have been generated [4,5]. MMMs combine the high selectivity of porous fillers with the ease of processability of the polymers to achieve an enhanced performance for various gas separations [6].

Among all kinds of fillers incorporated into the polymers to prepare MMMs, MOFs have been of great interest thanks to their high porosity, good mechanical, and thermal properties, along with their tunable pores and adsorption sites leading to superior gas separation performance [7]. Several MOF/polymer MMMs have shown to be promising for different separations, such as CO_2/CH_4, CO_2/N_2, H_2/CO_2, compared to the corresponding pure polymer membranes [8–12]. Incorporation of MOFs into polymers generally improves the gas permeability and/or the selectivity of the polymer membrane [13]. For instance, MOF-801/PIM-1 MMMs (PIM-1: polymer of intrinsic microporosity) having different filler loadings were fabricated and the results showed that the MMM having 5 wt.% MOF-801 loading has a significantly higher CO_2 permeability (9686 Barrer) compared to pure polymer (4200 Barrer), whereas the CO_2/N_2 selectivities (27) and O_2/N_2 selectivities (4.8) showed negligible improvement compared to pure polymer membrane having selectivities of 20 and 4, respectively [14]. In some cases, addition of MOFs into the polymers leads to reduced gas permeabilities. For example, CO_2 and H_2 permeabilities were reported to decrease from 10 to 5 Barrer and from 30 to 20 Barrer, respectively, when ZIF-8 was incorporated into Matrimid. However, these decreases in permeabilities were accompanied with improvements in H_2/CO_2 and CO_2/CH_4 selectivities from 40 to 121 and 124 to 472, respectively [15]. Achieving simultaneous improvement of selectivity and permeability by generating MMMs is highly desired and might be possible by incorporation of

* Corresponding authors at: Department of Chemical and Biological Engineering, Koc University, Rumelifeneri Yolu, 34450 Sariyer, Istanbul, Turkey.
E-mail addresses: auzun@ku.edu.tr (A. Uzun), skeskin@ku.edu.tr (S. Keskin).

https://doi.org/10.1016/j.seppur.2023.123346
Received 9 December 2022; Received in revised form 11 January 2023; Accepted 31 January 2023
Available online 4 February 2023
1383-5866/© 2023 The Author(s). Published by Elsevier B.V. This is an open access article under the CC BY-NC-ND license (http://creativecommons.org/licenses/by-nc-nd/4.0/).

novel filler materials into the polymers.

To obtain further improvement in the gas separation performance of MOFs, their modification with other functional materials to generate MOF-based composites has been suggested [16,17]. Ionic liquids (ILs) are molten salts made up of large organic cations with inorganic anions offering tunable physicochemical properties with almost unlimited structural variety [18]. Combining MOFs with ILs to enhance the gas separation performance of MOFs by modifying the MOFs' pore structure and facilitating CO_2 transport owing to the high solubility of CO_2 in most ILs has been reported [19]. Several studies demonstrated that the incorporation of ILs into MOFs to synthesize IL/MOF composites significantly improves the CO_2 selectivity of the parent MOF over N_2 and CH_4 [20–23]. Recently, IL/MOF composites have been incorporated as fillers into the polymers to fabricate IL/MOF/polymer MMMs, enhancing the CO_2 affinity and molecular sieving properties of the membranes, resulting in MMMs with improved permeability and selectivity [14,24–28]. For instance, IL/ZIF-8 composite having 1-butyl-3-methylimidazolium bis(trifluoromethylsulfonyl)imide, [BMIM][Tf_2N], as the IL was synthesized and incorporated into Pebax [29]. The results showed that CO_2/CH_4 and CO_2/N_2 selectivities of the MMM having 15 wt.% IL/ZIF-8 composite were (34 and 84, respectively) higher than the selectivities of pure Pebax membrane (28 and 40, respectively). In another example, IL/ZIF-8 composite prepared by using a different IL, 1-*n*-butyl-3-methylimidazolium hexafluorophosphate, [BMIM][PF_6], incorporated into Pebax at a loading of 25 wt.% [30]. The resulting MMM showed a higher CO_2 permeability (120 Barrer) and CO_2/N_2 selectivity (90) than the pure polymer membrane (59 Barrer and 55, respectively).

Recently, IL/MOF composites with amine-functionalized ILs and MOFs have been incorporated into different polymers. For instance, [NH_2-PMIM][Tf_2N]/ZIF-67 composite ([NH_2-PMIM][Tf_2N]: 1-aminopropylimidazolium bis(trifluoromethylsulfonyl)imine) was prepared and incorporated in the PIM-1 polymer [31]. The results showed that with 5 wt.% IL/MOF loading, CO_2 permeability of the MMM was almost double (7190 Barrer) of the polymer (4310 Barrer) with unchanged CO_2/N_2 selectivity (22). In another study, [BMIM][Tf_2N]/NH_2-MIL-101(Cr)/Matrimid MMM with a filler loading of 7 wt.% was synthesized [32]. Both the CO_2 permeability and CO_2/CH_4 selectivity were improved from 6 to 19 Barrer and from 35 to 113, respectively, compared to corresponding values of pure Matrimid. Similarly, [C_3NH_2bim][Br]/NH_2-MIL-101(Cr) ([C_3NH_2bim][Br]: 1-butylimidazole 2-bromopropylamine hydrobromide) composite was incorporated into PIM-1 [33] and the CO_2 permeability of IL/MOF/PIM-1 MMM with 5 wt.% IL/MOF loading (3000 Barrer) was approximately 1.3-times higher than that of PIM-1 membrane (2400 Barrer). The CO_2/N_2 selectivity (27), on the other hand, was almost 1.6-times higher than the polymer (17).

All these studies demonstrate that the MMMs prepared by incorporation of IL/MOF composites into polymers offer significantly better separation performance than the pure polymer membrane. There exists a very large number and variety of ILs (in the order of 10^{18}) [34] and MOFs (114,373) [35] yielding in the order of 10^{23} different IL/MOF composite possibilities, however, the number of reported MMMs having IL/MOF composite as a filler is very limited and most of the studies focused on ILs having imidazolium-based cations. Recently, we showed that incorporating a pyrrolidinium-based IL, namely 1-*n*-butyl-1-methylpyrrolidinium dicyanamide, [BMPyrr][DCA], into UiO-66 to synthesize an IL/MOF composite resulted in exceptionally improved CO_2/N_2 and CH_4/N_2 adsorption selectivities [36]. However, we have no information about the potential impact of using a pyrrolidinium-based IL/MOF composite as the filler on the CO_2 separation performance of the resulting MMM.

In this work, we synthesized highly CO_2-selective IL/MOF/polymer MMMs for CO_2/N_2 and CO_2/CH_4 separations by specifically choosing a pyrrolidinium-based IL, 1-methyl-1-propyl pyrrolidinium dicyanamide ([MPPyr][DCA]), to prepare a novel IL/MOF composite. [MPPyr][DCA] was selected as an IL because of the high CO_2 solubility of $[DCA]^-$ anion along with pyrrolidinium cation offering superior gas separation properties and less toxicity compared to the imidazolium-based ILs [37]. [MPPyr][DCA] has not been reported in the form of IL-incorporated MOF filler in previous MMM studies. Thus, to unlock the potential of this IL as a composite filler in MMM applications by extending the list of pyrrolidinium-based ILs is highly desired to understand its potential for improved separation performance of the MMMs. MIL-101(Cr) was selected as the host MOF since it has a high surface area and unsaturated Cr(III) sites offering strong Lewis acid-base interactions with the oxygen of CO_2, leading to high CO_2 adsorption [38,39]. [MPPyr][DCA]/MIL-101(Cr) composite having 45 wt.% IL was synthesized via wet impregnation method and incorporated into Pebax polymer as the filler to fabricate [MPPyr][DCA]/MIL-101(Cr)/Pebax MMMs with filler loading of 10, 15, and 20 wt.%. This is the first attempt to study the effect of using pyrrolidinium-based IL/MOF composite as the filler on the separation performance of a polymer membrane. Moreover, MIL-101(Cr)/Pebax MMMs and [MPPyr][DCA]/Pebax MMMs were also synthesized for comparison. The structural characteristics and the molecular interactions between the individual components of the MMMs were characterized in detail and their influences on the CO_2/N_2 and CO_2/CH_4 separation performances of the resulting MMMs were comprehensively investigated. Our results showed that [MPPyr][DCA]/MIL-101(Cr)/Pebax MMMs offer comparable CO_2 permeability with exceptionally high CO_2/N_2 ideal selectivity compared to the previously reported IL/MOF/polymer MMMs in the literature. These results will guide the design of new IL/MOF/polymer MMMs having extraordinarily high performances for CO_2 separations.

2. Materials and methods

2.1. Materials

Pebax 1657 polymer (containing 60 wt.% polyethylene oxide (PEO) and 40 wt.% polyamide (PA)) was kindly provided by Arkema (Italy). MIL-101(Cr) was purchased from Nanoshel, UK, [MPPyr][DCA] (>98 %) was bought from Iolitec, ethanol, and acetone (analytical grade) were bought from Sigma-Aldrich. Each chemical was stored in an argon-filled Labconco glovebox prior to use. CO_2 (99.9 %), CH_4 (99.9 %), N_2 (99.998 %), and He (99.999 %) were purchased from Air Liquide.

2.2. Synthesis of IL/MOF composite

Pristine MIL-101(Cr) was activated at 125 °C under vacuum before the IL incorporation. [MPPyr][DCA]/MIL-101(Cr) composite was prepared using wet impregnation method [19,23]. First, 0.45 g of IL with a target loading of 45 wt.% in the IL/MOF composite was dissolved in 20 mL of acetone and left for stirring for 1 h. Then, 0.55 g of activated MIL-101(Cr) was added in the IL solution and kept under stirring at 35 °C in an open atmosphere until the solvent was completely evaporated. The resulting sample was further dried overnight in oven at 80 °C to obtain the [MPPyr][DCA]/MIL-101(Cr) composite.

2.3. Fabrication of MMMs

Pure Pebax membrane, MOF/polymer MMMs and IL/MOF/polymer MMMs were prepared via conventional solution-casting method. Polymer pallets, MOF particles, and IL/MOF composite were dried overnight at 80 °C prior to membrane fabrication. For pure Pebax membrane, 4 wt.% of polymer solution was prepared by dissolving Pebax in water/ethanol (30/70 wt.%) mixture and it was continuously stirred for 4 h at 80 °C. Afterwards, the polymer solution was casted on a Teflon petri dish and covered with inverted funnel to slowly evaporate the solvent at room temperature for 24 h. Finally, for the complete removal of solvent, the membrane was placed in oven overnight at 65 °C.

MOF/polymer MMMs were prepared by mixing 10, 15, and 20 wt.% of vacuum-dried MIL-101(Cr) particles into ethanol/water solvent

mixture followed by continuous stirring for 4 h. Afterwards, the MOF solutions were sonicated for 30 min to ensure the well-dispersion of the particles and then they were added into the Pebax solution (4 wt.%), prepared by continuous stirring for 4 h at 80 °C in ethanol/water mixture. Next, the MOF/polymer solutions were placed in an ultrasonic bath for 30 min to prevent agglomeration of the particles. The resultant solutions were continuously stirred for 4 h and then casted on a Teflon substrate.

To fabricate the IL/MOF/polymer MMMs with 10, 15, and 20 wt.% IL/MOF loadings, a similar procedure was followed. The desired loading of IL/MOF filler was dispersed in ethanol/water solvent mixture, stirred for 4 h, followed by 30 min of ultra-sonication. Finally, the sonicated IL/MOF solution was mixed with the Pebax solution, sonicated (30 min), stirred (4 h) and, casted on a Teflon substrate. The controlled evaporation of the solvent was carried out for all membranes by placing an inverted funnel on the petri dishes for 24 h. To check the possibility of leaching out of the IL during the mixing process, the IL/MOF suspension was dried overnight at 80 °C and IR spectra of the dried composite was recorded. Detailed discussion on these measurements is presented in the characterization section and additional data are provided in **Fig. S1** of the Supplementary data (SD).

To compare the separation performance of the best performing IL/MOF/polymer MMM, two other MMMs, IL/Pebax MMM (following the same procedure as MOF/polymer MMMs described above) and free-IL/free-MOF/Pebax MMM were synthesized. For free-IL/free-MOF/Pebax MMM, a certain amount of IL and MOF was added to the ethanol/water solution and stirred for 4 h, then the suspension was added to the Pebax solution followed by another 4 h stirring. Finally, membranes were dried in an oven overnight at 65 °C and stored in a desiccator. The thickness of all MMMs was in the range of 90–110 μm as measured by a digital slide caliper.

2.4. Characterization techniques

Brunauer-Emmett-Teller (BET) measurements were performed to determine the surface area and pore volume of the pristine MOF and IL/MOF composite using a Micromeritics ASAP 2020 adsorption analyzer. MOF and IL/MOF composite particles were activated at 150 °C under vacuum for 12 h prior to the measurements. Afterwards, N_2 adsorption isotherms were obtained at 78 K from 10^{-6} to 1 bar. The BET equation and the *t*-plot method were used to calculate the surface area and pore volume in a relative pressure range of 0.05–0.65 (P/P_o), respectively. Scanning electron microscopy (SEM) images of the MOF, IL/MOF composite, and all the MMMs were obtained by using a Zeiss Evo LS 15 electron microscope operating under ultra-high vacuum conditions with an accelerating voltage of 20 kV. To obtain the cross-sectional images of MMMs, the samples were prepared by freeze cutting under liquid N_2, followed by gold coating.

X-ray diffraction (XRD) data of the pristine MIL-101(Cr), [MPPyr][DCA]/MIL-101(Cr) composite, and all the MMMs were recorded using a Bruker D2 Phaser instrument. A Cu-Kα radiation with wavelength of 1.54060 Å was used to collect data in the 2θ range between 5 and 50° with a step size of 0.0204°. Thermogravimetric analysis (TGA) measurements were conducted using a TA Instruments Q500 analyzer. For the MMMs, the experiments were performed at a heating rate of 10 °C min^{-1}, starting from room temperature up to 800 °C. All the measurements were conducted under N_2 flow as balance and purge gas at a flow rate of 40 and 60 mL/min, respectively. To analyze the thermal stability of the samples, the onset (T_{onset}) and derivative onset (T'_{onset}) temperatures were determined from the thermogravimetric (TG) and derivative TG (DTG) curves, respectively. In this study, the T'_{onset} values were considered as the initial thermal decomposition temperature, because the T_{onset} values generally overestimate the decomposition temperatures [40]. IR spectra of the samples were collected using a Bruker Vertex 80v spectrometer in the range of 400 to 4000 cm^{-1} in transmittance mode at a spectral resolution of 2 cm^{-1}. IR bands deconvolution was performed using Fityk software by employing the Voigt function [41]. COnductor-like Screening MOdel for Realistic Solvents (COSMO-RS) calculations were performed to calculate the solubilities of CO_2, N_2, and CH_4 in bulk [MPPyr][DCA] between a pressure range of 0.1 and 1 bar [39]. COSMOThermX software (version:C30_160) was employed with respective triple-z valence polarized basis set (TZVP-FINE) parameterizations to perform these calculations.

2.5. Gas adsorption measurements

Volumetric gas adsorption measurements of pristine MIL-101(Cr) and IL-incorporated MIL-101(Cr) composite were performed for CO_2, CH_4, and N_2 using a Quantachrome iSorb HP2 volumetric gas adsorption analyzer. Adsorption isotherms for each gas were obtained at 25 °C in a pressure range of 0.001–1 bar. Approximately, 0.4 g of the samples were used for each measurement, which were degassed at 125 °C for 12 h under a high vacuum prior to the measurements. To compare the gas separation performance of the pristine MIL-101(Cr) and [MPPyr][DCA]/MIL-101(Cr) composite, each gas adsorption isotherm was fitted to the Dual-site Langmuir-Freundlich model by using Ideal Adsorbed Solution Theory $(IAST)^{++}$ software [42] and the corresponding fitting parameters were given in **Table S1**.

2.6. Gas permeation experiments

Single-component CO_2, CH_4, and N_2 permeability measurements were conducted at 1 bar and 35 °C, using a custom-built constant pressure/variable volume setup as shown in **Fig. S2**. Helium was used as a sweep gas in the setup for all measurements. Each MMM was tested three-times and the average permeabilities and selectivities were reported along with the corresponding standard deviation. The MMMs were supported on porous stainless-steel module having an effective surface area of 7 cm^2 and were tightly sealed by rubber O-rings. Electronic mass flow controllers (MFCs, Alicat) and a back pressure regulator (BPR, Equilibar) were employed to adjust the flowrate and the upstream pressure of each gas, respectively. BPR maintained the upstream pressure at 1 bar (gauge pressure) and the downstream pressure was under atmospheric conditions. During and after the measurements, the permeation unit was continuously purged with He as a sweep gas. The permeate gas composition was determined by a Hiden Analytical mass spectrometer (QGA gas analyzer) equipped with a quadrupole mass filter and a heated sampling capillary. Based on the mass spectrometric analysis of the permeate and sweep gas streams, gas fluxes were calculated from the sweep gas flow rate. The permeability (Barrer) of the gas 'a', P_a was calculated by using the equation (1), where J_a is the flux (cm^3(STP)/(s.cm^2)). J_a is defined as the flowrate (cm^3(STP)/s) of the gas, Q_a, divided by the unit area (cm^2), A, of the membrane.ΔP (cm Hg) is the pressure difference across the membranes, and l (cm) is the membrane thickness:

$$P_a = (J_a/\Delta P) \times l \quad (1)$$

The ideal selectivity of the membrane ($S_{a/b}$) was calculated by dividing the permeability values measured for different gases using equation (2), where *a* and *b* are two different gases:

$$S_{a/b} = P_a/P_b \quad (2)$$

3. Results and discussion

3.1. Characterization of the materials

3.1.1. Pristine MOF and IL/MOF composite

The IL loading in the as-synthesized [MPPyr][DCA]/MIL-101(Cr) composite was determined by washing the composite several times with acetone, which was chosen as the solvent because it can enter the pore window of MIL-101(Cr) (16 Å) [12] to remove any incorporated IL

molecules. After washing, the filtrate was collected in a vial and the washed IL/MOF composite was dried overnight at 80 °C. The IR spectra of the dried composite, the filtrate, and the bulk IL are presented in **Fig. S3**. Data showed that the IL was completely removed from the composite upon washing. By measuring the amount of the dried sample, the IL loading was determined as approximately 41 wt.%, which is slightly less than the stoichiometric IL loading of 45 wt.% targeted to prepare the [MPPyr][DCA]/MIL-101(Cr) composite. This difference can be attributed to the loss of some [MPPyr][DCA] on the walls of the container during the synthesis of the composite.

SEM images of the pristine MIL-101(Cr) and [MPPyr][DCA]/MIL-101(Cr) composite (Fig. 1**a-b** and Fig. 1**c-d**, respectively) were obtained to examine the effect of IL incorporation on the morphology of the pristine MOF. SEM images of the composite given in Fig. 1**c-d** showed the octahedral structure of MIL-101(Cr). Thus, the crystal morphology of the MIL-101(Cr) was well-preserved upon the incorporation of [MPPyr][DCA]. Moreover, it was also observed that the surface morphology of the MOF was not affected by the addition of IL, and no external layer formation was visible in the SEM images, implying that the IL was successfully incorporated inside the MIL-101(Cr) cages.

The N_2 adsorption isotherms obtained at the liquid nitrogen temperature on the pristine MIL-101(Cr) and [MPPyr][DCA]/MIL-101(Cr) composite are presented in Fig. 2**a**. Moreover, pore size distribution analysis was made for the pristine MIL-101(Cr) as given in **Fig. S4**. Data presented in Fig. 2**a** showed that the surface area and pore volume of [MPPyr][DCA]/MIL-101(Cr) were significantly lower than those of pristine MIL-101(Cr). Upon the incorporation of [MPPyr][DCA], the surface area and pore volume of MIL-101(Cr) decreased from 1924 m^2/g and 0.6 cm^3/g to 109 m^2/g and 0.08 cm^3/g, respectively. This decrease can be attributed to the pore occupation of MIL-101(Cr) with the IL molecules, resulting in a lowering in the N_2 uptakes, consistent with the literature [36]. Accordingly, N_2 solubility in bulk [MPPyr][DCA] was calculated by the COSMO-RS calculations as presented in **Fig. S5**, which showed that IL has a poor solubility for N_2 at the BET measurement conditions. Therefore, due to low N_2 solubility of [MPPyr][DCA], the pores of MIL-101(Cr) are mostly unavailable for N_2 especially if the IL molecules are present at their pore openings [43]. Hence, the BET results are not considered to be very reliable in providing precise surface area and pore volume of IL/MOF composites, however, they indicate the successful incorporation of the IL.

Consistently, the XRD patterns presented in Fig. 2**b** showed that there are no significant changes in the diffraction peaks of MIL-101(Cr) and [MPPyr][DCA]/MIL-101(Cr) composite. Specifically, the sharp peaks located at $2\theta = 8.4$, 9.0, and 16.5°, corresponding to the main diffraction peaks of MIL-101(Cr) [44], remained intact in IL-incorporated MOF composite, confirming that the crystal structure of the MIL-101(Cr) was preserved upon the incorporation of IL. However, some changes in the intensities of the peaks present in [MPPyr][DCA]/MIL-101(Cr) composite were observed compared to those on the pristine MIL-101(Cr). These differences can be attributed to a possible change in the electronic structure or the preferential orientation of the MOF crystals, because of the incorporation of IL molecules inside the MOF's pores, consistent with earlier reports [45].

The TGA analysis was conducted for pristine MIL-101(Cr) and [MPPyr][DCA]/MIL-101(Cr) as shown in Fig. 2**c**. The measurements were started after the complete evaporation of moisture content and any residual solvent present in the samples at 130 °C. The results showed that MIL-101(Cr) starts to decompose at a T'_{onset} value of approximately 330 °C, which can be attributed to the decomposition of the organic ligand present in the MOF structure [46]. The T'_{onset} value of bulk [MPPyr][DCA] was found to be 230 °C, whereas for IL/MOF composite, T'_{onset} value was around 300 °C. These results showed that the T'_{onset} of the as-synthesized IL/MOF composite is lower than that of the pure MOF, which can be associated with the presence of direct IL-MOF interactions in the composite. These interactions changed the MOF composite's decomposition mechanism (from one to multiple steps) and decreased the thermal stability limits of the IL/MOF composite as compared to the pristine MOF [47].

To have insights into the IL-MOF interactions, IR analysis was performed on the MIL-101(Cr), bulk [MPPyr][DCA], and the [MPPyr][DCA]/MIL-101(Cr) composite as shown in Fig. 2**c**. In the IR spectrum of [MPPyr][DCA], the peaks located at 2881 and 2972 cm^{-1} were assigned to the symmetric and asymmetric ν(C—H) vibrations on the IL's cation, respectively, whereas the IR bands at 1301, 2123, 2189, and 2223 cm^{-1} were attributed to ν(C≡N) vibrations of the $[DCA]^-$ anion [48]. It was observed that ν(C≡N) characteristic vibrations of the

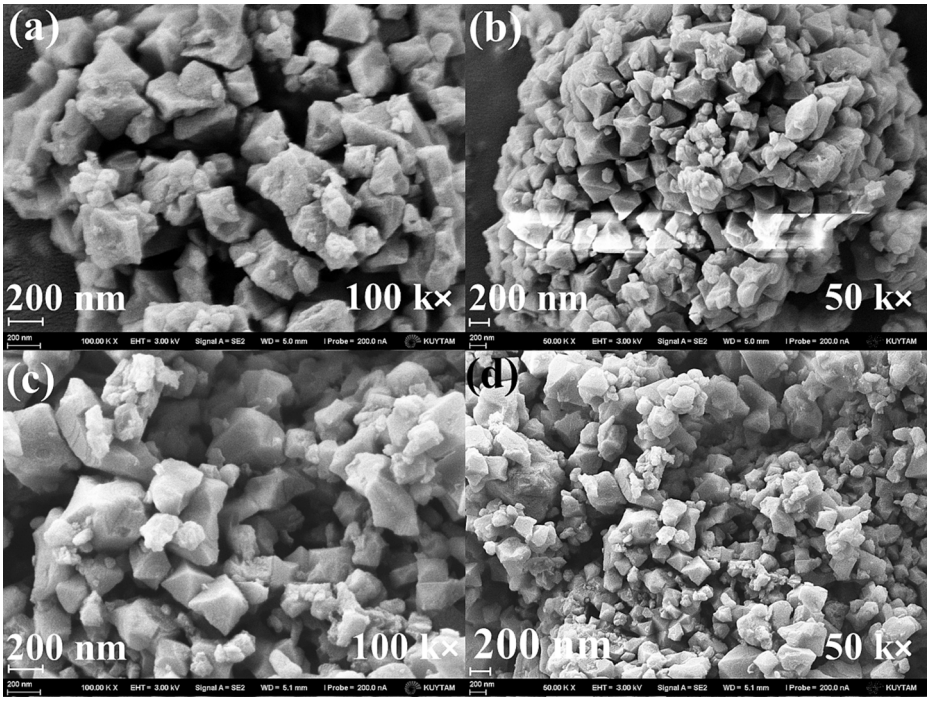


Fig. 1. SEM images of (a, b) MIL-101(Cr) and (c, d) [MPPyr][DCA]/MIL-101(Cr) composite obtained at magnifications 100× and 50 k×.

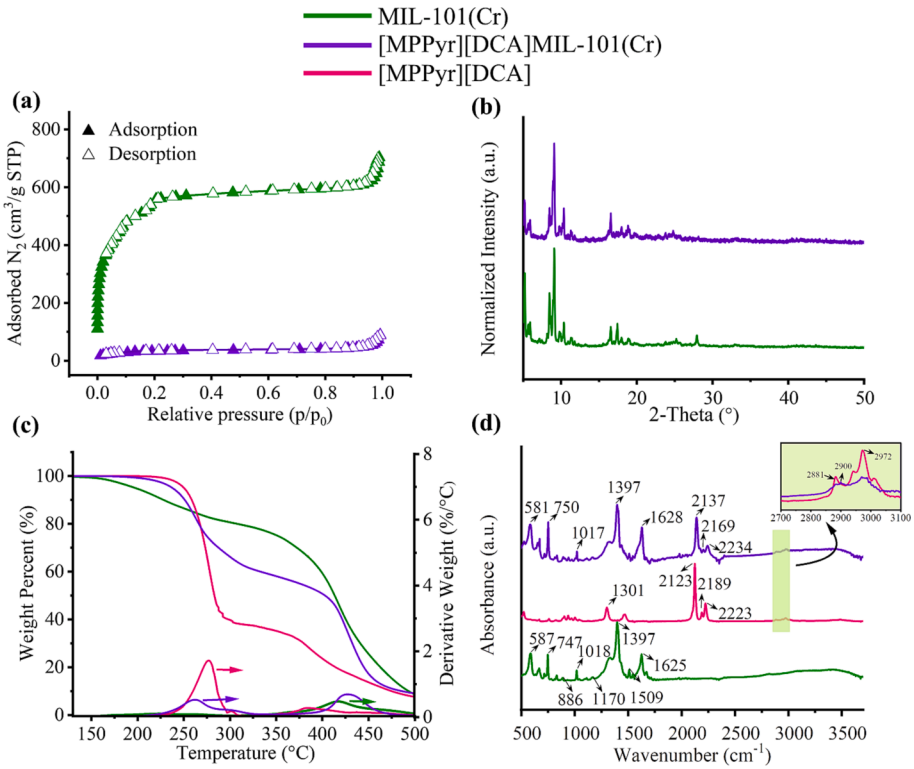


Fig. 2. (a) N_2 adsorption–desorption isotherms, (b) XRD diffractogram, (c) TGA curves, (d) IR spectra of pristine MIL-101(Cr), bulk [MPPyr][DCA], and [MPPyr][DCA]/MIL-101(Cr) composite.

$[DCA]^-$ anion exhibited blue-shifts of 14 and 11 cm^{-1}, in the spectrum of the composite, respectively. Moreover, data further indicated that the characteristic ν(C—H) peak located at 2881 cm^{-1} blue-shifted to 2900 cm^{-1} upon the incorporation of the IL into the MOF. ———

In the lower frequency region of the IR spectrum of the pristine MIL-101(Cr), the band at 587 cm^{-1} was associated with the coordination of 1,4-benzene dicarboxylate (BDC) linker to the chromium sites. Besides this feature, the bands located between 600 and 1630 cm^{-1} were attributed to the benzene ring, including the stretching ν(C═C) vibrations at 1509 cm^{-1} and ν(C—H) vibrations at 747, 886, 1018, and 1170 cm^{-1} [49]. Furthermore, the peaks located at 1397 and 1625 cm^{-1} corresponded to the symmetric ν(COO) and asymmetric ν(C—O) vibrations of dicarboxylate groups in the BDC linker, respectively [50]. Upon the incorporation of IL into the MIL-101(Cr), characteristic ν(Cr–O) peak of the MIL-101(Cr) located at 587 cm^{-1} presented a red-shift of 6 cm^{-1}, while the peaks at 747 and 1625 cm^{-1} exhibited blue-shifts of 3 cm^{-1}. These shifts in the characteristic ν(Cr–O) band of pristine MIL-101(Cr) indicate the Cr nodes of the MOF strongly interacts with the anion of the IL. The changes in the characteristic peak positions of anion of the IL suggest that the interionic interaction between anion and cation of IL

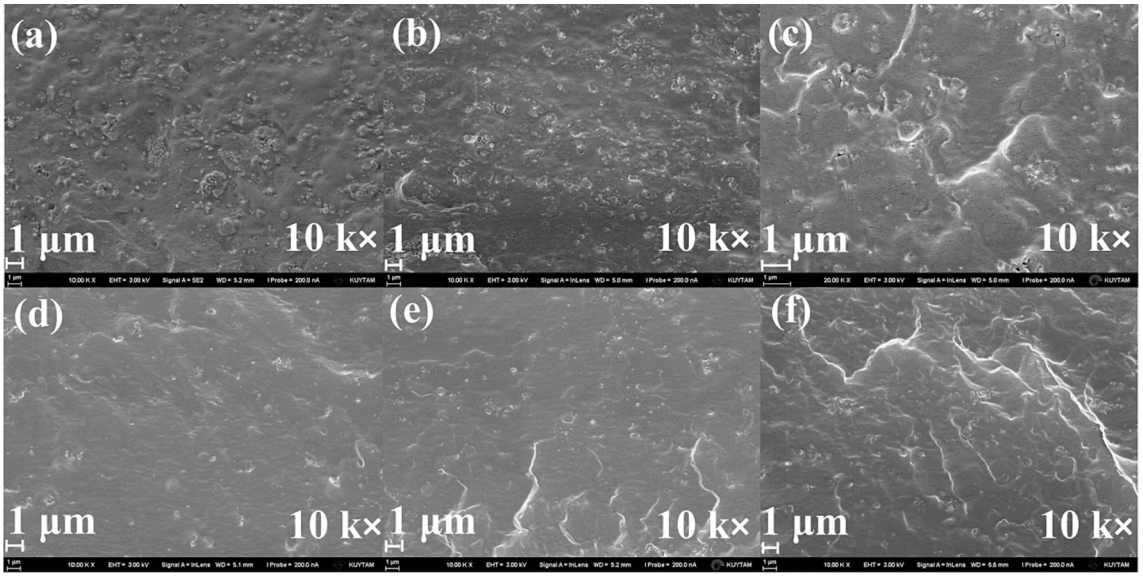


Fig. 3. Cross-sectional SEM images of MIL-101(Cr)/Pebax MMMs with (a) 10 wt.%, (b) 15 wt.%, (c) 20 wt.% MIL-101(Cr) loadings and [MPPyr][DCA]/MIL-101(Cr)/Pebax MMMs with (d) 10 wt.%, (e) 15 wt.%, (f) 20 wt.% [MPPyr][DCA]/MIL-101(Cr) loadings.

weakens as it interacts more with the metal nodes of MIL-101(Cr). Hence, the electronic environment of the MOF structure changes upon the IL incorporation because of the existence of direct interactions between IL (anion) and MOF.

3.1.2. MOF/polymer and IL/MOF/polymer MMMs

Cross-sectional SEM images of all MMMs were obtained to investigate the changes in the morphologies of MMMs upon the incorporation of the filler. The images of MIL-101(Cr)/Pebax MMMs represented in Fig. 3**a-c** and [MPPyr][DCA]/MIL-101(Cr)/Pebax MMMs presented in Fig. 3**d-f** showed obvious differences in the morphology of two types of the membranes. As the loadings of MOF and IL/MOF fillers were increased, the MMMs showed less-smooth structure, especially the ones containing 20 wt.% filler. In the case of the MIL-101(Cr)/Pebax MMM with 20 wt.% MOF loading, agglomeration of particles was clearly observed, which can be attributed to the poor compatibility between MOF and polymer especially at higher loadings. The comparison between IL/MOF/polymer and MOF/polymer MMMs, on the other hand, revealed that IL addition improved the filler/polymer compatibility resulting in more uniform and homogenous distribution of the filler at all loadings. This improvement suggests that IL molecules might be partially leaching out from the MOF cages in the presence of the solvent (ethanol/water mixture) during the synthesis of MMMs. To confirm this possibility, we washed the IL/MOF composite in ethanol/water mixture and checked the IR spectra of both the washed sample and the filtrate. The data presented in **Fig. S1** demonstrated that some IL molecules leached out from the cages of MOF. Hence, we infer that IL molecules might be present both inside and outside of the MOF in the composite. The presence of IL on the external surface of the MOF improves the compatibility of the filler with the polymer matrix [51]. Details are presented in the discussion of IR results.

The XRD analyses of the pure Pebax, MIL-101(Cr)/Pebax, and [MPPyr][DCA]/MIL-101(Cr)/Pebax MMMs with 10, 15, and 20 wt.% fillers were performed to study the structural properties of MMMs as shown in Fig. 4**a-g**. For the pure Pebax membrane, a broad peak present at $2\theta = 13\text{-}23^{\circ}$ corresponded to the polyamide (PA) segment [52], which was also observed in the XRD data of all the prepared MMMs without any change in its peak position. In the XRD patterns of MMMs some new peaks were observed at $2\theta = 8.6$, 9.0, and 16.8°, which were attributed to the characteristic peaks of the pristine MIL-101(Cr). In the case of MIL-101(Cr)/Pebax MMMs, Fig. 4**b-d**, the intensities of characteristic MIL-101(Cr) peaks were observed to increase as the filler loading was increased from 10 to 20 wt.%, indicating the high crystallinity of the MMMs at higher MOF loadings. However, the relative intensity of characteristic diffraction peaks of MIL-101(Cr) was reduced in all the IL/MOF/polymer MMMs as shown in Fig. 4**e-g**, which can be ascribed to the lower loading (wt.%) of MIL-101(Cr) in IL/MOF composite incorporated into the Pebax to form the MMMs. Moreover, the intersegmental distance, known as *d*-spacing, between the polymer chains was also calculated from the Bragg's equation for all the MMMs synthesized in this work. The results are presented in **Table S2**. As, it can be seen from the Fig. 4 the characteristic peaks of the Pebax showed no significant change in the 2-theta values, therefore the *d*-spacing of the polymer chains in the MMMs showed slight changes. Moreover, the [MPPyr][DCA]/MIL-101(Cr)/Pebax MMMs showed smaller *d*-spacings values, which can be attributed to the interactions of the [MPPyr][DCA]/MIL-101(Cr) composite with the polymer, while MIL-101(Cr)/Pebax MMMs were characterized with slightly higher *d*-spacings values resulting in slightly high gas permeabilities.

The TGA curves of MIL-101(Cr)/Pebax MMMs and [MPPyr][DCA]/MIL-101(Cr)/Pebax MMMs at different filler loadings are shown in Fig. 5. It was observed that decomposition temperature of MMMs did not have any noticeable difference and all displayed one-step decomposition mechanism. Accordingly, the weight loss observed at approximately 350 and 360 °C in the TGA curves of MIL-101(Cr)/Pebax MMMs and [MPPyr][DCA]/MIL-101(Cr)/Pebax MMMs, respectively, indicated the decomposition of the polymer backbone present in the MMMs. A slight increase (higher than the error range of the measurements, ±5 °C) in the decomposition temperature of IL/MOF/polymer MMMs as compared to MIL-101(Cr)/Pebax MMMs indicated a slight improvement in the thermal stability of MMMs, most probably associated with the incorporation of IL/MOF composite filler into the polymer [53]. Generally, none of the MMMs synthesized in this work show significant weight loss up to 340 °C, indicating a high thermal stability of the MMMs.

FTIR spectra of the pure Pebax, MIL-101(Cr)/Pebax MMMs, and [MPPyr][DCA]/MIL-101(Cr)/Pebax MMMs are represented in Fig. 6**a-g**. The IR spectrum represented as Fig. 6**a**, corresponds to the pure Pebax membrane, showed the characteristic band of PEO segment at 1100 cm^{-1} representing the ν(C—O—C) group [54], whereas the peaks located at 1637, 1732, and 3297 cm^{-1} belong to PA segment of Pebax, attributed to the ν(O—C—O) group, ν(H—N—C═O) group [55], and ν(N—H) group [56], respectively. The IR spectra of MMMs given in Fig. 8**b-g** showed the similar characteristic IR peaks of Pebax. In the case of MIL-101(Cr)/Pebax MMMs having 10 wt.% MIL-101(Cr) loading,

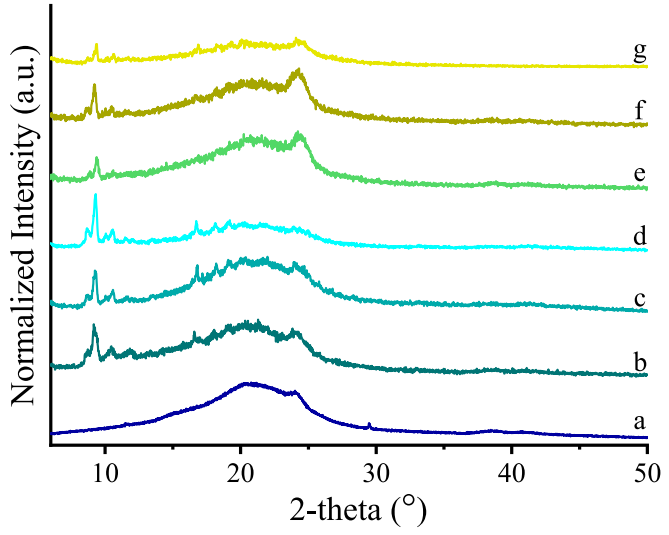


Fig. 4. XRD spectra of membranes. Pure Pebax (a), MIL-101(Cr)/Pebax MMMs with 10 wt.% (b), 15 wt.% (c), 20 wt.% (d) MIL-101(Cr) loadings. [MPPyr][DCA]/MIL-101(Cr)/Pebax MMMs with 10 wt.% (e), 15 wt.% (f), 20 wt.% (g) [MPPyr][DCA]/MIL-101(Cr) loadings.

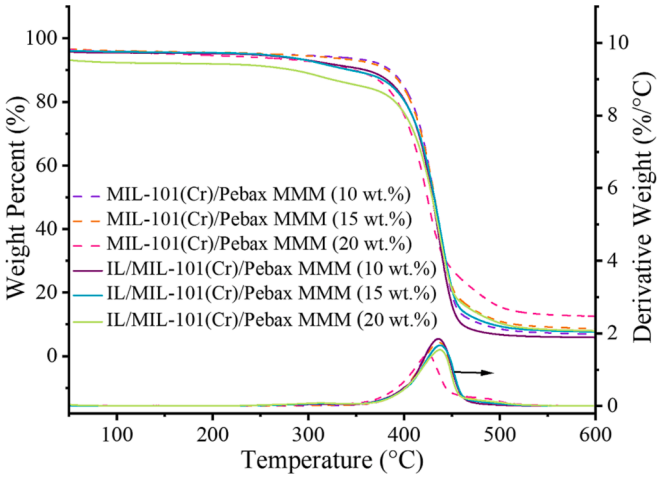


Fig. 5. TGA and DTG curves of MIL-101(Cr)/Pebax MMMs and [MPPyr][DCA]/MIL-101(Cr)/Pebax MMMs with 10 wt.%, 15 wt.% and, 20 wt.% MIL-101(Cr) loadings and [MPPyr][DCA]/MIL-101(Cr) composite loadings respectively.

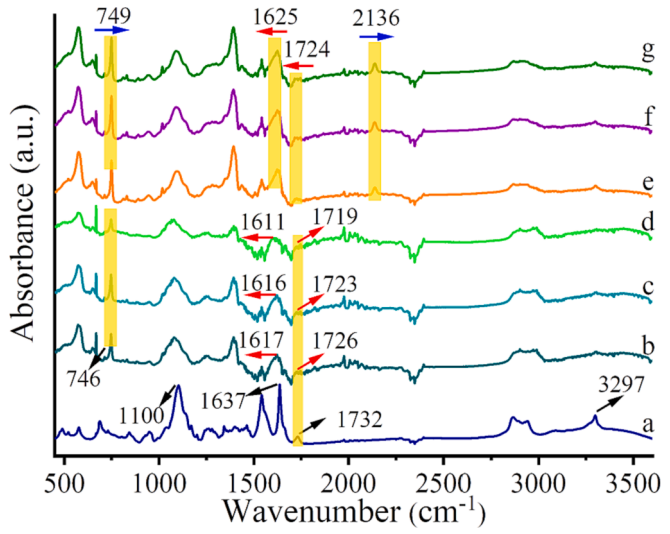


Fig. 6. IR spectra of the membranes. Pure Pebax (a), MIL-101(Cr)/Pebax MMMs with 10 wt.% (b), 15 wt.% (c), 20 wt.% (d) MIL-101(Cr) loadings, and [MPPyr][DCA]/MIL-101(Cr)/Pebax MMMs with 10 wt.% (e), 15 wt.% (f), 20 wt.% (g) [MPPyr][DCA]/MIL-101(Cr) loadings.

Fig. 6**b**, the corresponding Pebax bands were located at 1080 cm^{-1} (ν(C—O—C)), 1617 cm^{-1} (ν(O—C—O)), 1726 cm^{-1} (ν(H—N—C═O)), and 3295 cm^{-1} (ν(N—H)). As the loading of MIL-101(Cr) was increased in the polymer matrix to 15 and 20 wt.% (Fig. 6**c-d**), both of the ν(C—O—C) and ν(O—C—O) bands exhibited red-shifts of 8 cm^{-1} , while the position of the ν(H—N—C═O) band was red-shifting by 7 cm^{-1}, indicating the presence of MOF/polymer interaction. Moreover, new IR bands were observed at 575, 746, and 1393 cm^{-1} are associated with the ν(Cr—O), ν(C—H), and ν(COO) groups present in MIL-101(Cr) structure.

The IR spectra of the IL/MOF/polymer MMMs are represented in Fig. 6**e-g**, with characteristic Pebax peaks located at 1093 cm^{-1} (ν(C—O—C)), 1625 cm^{-1} (ν(O—C—O)), 1724 cm^{-1} (ν(H—N—C═O)), and 3299 cm^{-1} (ν(N—H)). Red-shifts of 7, 12, and 9 cm^{-1} were observed in ν(C—O—C), ν(O—C—O), and ν(H—N—C═O) bands, respectively, whereas ν(N—H) peak showed a slight blue-shift as compared to its position on the pure Pebax membrane. However, with an increase in IL/MOF composite loadings, no significant changes in the IR bands of Pebax groups were observed (Fig. 6**e-g**). The characteristic band corresponding to MIL-101(Cr) observed at 746 cm^{-1} exhibited a slight blue-shift of 3 cm^{-1} in the IR bands of IL-modified MMMs. The strong shifts in the peak positions of the polymer functional groups and the ν(Cr—O) band present in [MPPyr][DCA]/MIL-101(Cr), are attributed to the strong interaction between the IL/MOF composite and Pebax polymer. Moreover, a new peak was also observed at 2136 cm^{-1}, corresponding to the ν(C≡N) vibrations of $[DCA]^-$ anion present in the IL. The corresponding peak showed a blue-shift of 13 cm^{-1} as compared to its position (2123 cm^{-1}) in [MPPyr][DCA]/MIL-101(Cr) composite spectra as shown in Fig. 2**c**. The significant shift in the IL peak indicated the strong interactions present between the IL and the polymer matrix. To further validate these IL/polymer interactions, as discussed briefly above, we recorded the IR spectra of [MPPyr][DCA]/MIL-101(Cr) composite mixed in ethanol/water solution prior to membrane synthesis shown in **Fig. S1**. It was observed that the intensity of IL peaks in the sample after mixing in ethanol/water mixture solution were decreased. This can be attributed to the fact that the pore window of MIL-101(Cr) (~16 Å) is larger as compared to the size of solvent molecules, ethanol (4.5 Å) and water (2.3 Å) [57], which can enter the pores of MIL-101(Cr). Based on these results, it can be inferred that some of the IL molecules left the pores of MIL-101(Cr) and were freely dispersed in the polymer matrix during the membrane synthesis. Hence, the bulk [MPPyr][DCA] strongly interacted with the Pebax, which is consistent with the IR spectra of [MPPyr][DCA]/MIL-101(Cr)/Pebax MMMs. Moreover, the presence of these IL molecules in the polymer matrix enhances the MIL-101(Cr)/polymer interfacial compatibility which can lead to improved gas separation performance of MMMs [51], discussed in the following section.

3.2. Gas separation performances of materials

3.2.1. Adsorption-based separation with MOF and IL/MOF composite

Volumetric gas uptakes of CO_2, N_2, and CH_4 in MIL-101(Cr) and [MPPyr][DCA]/MIL-101(Cr) composite were measured at 25 °C and 1 bar as shown in Fig. 7**a**, to study the effect of IL incorporation on the gas separation performance of MIL-101(Cr). Adsorption isotherms were

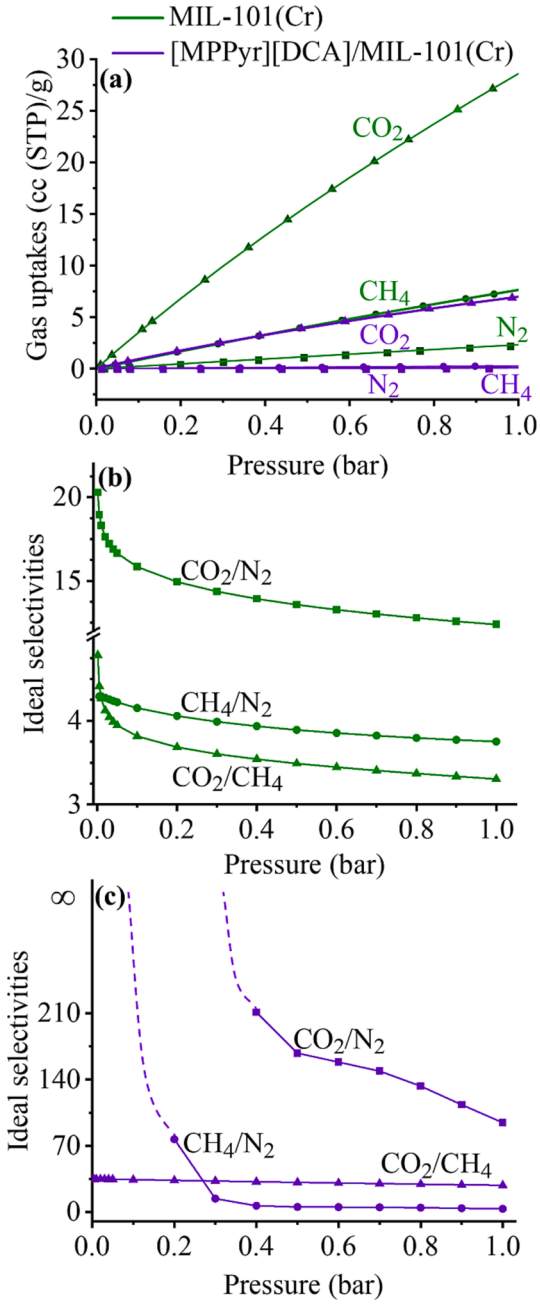


Fig. 7. (a) Gas adsorption uptakes of MIL-101(Cr) and [MPPyr][DCA]/MIL-101(Cr) composite, (b) ideal adsorption selectivities of MIL-101(Cr), (c) ideal adsorption selectivities of [MPPyr][DCA]/MIL-101(Cr) composite. The dotted lines in (c) represent practically infinite selectivities as the N_2 uptakes become unmeasurable at these pressures.

fitted to the dual-site Langmuir-Freundlich (DSLF) model to compare the separation performance of MIL-101(Cr) and [MPPyr][DCA]/MIL-101 (Cr) composite and the corresponding fitting parameters were given in **Table S1**. CO_2, N_2, and CH_4 uptakes of IL/MOF composite were less than the corresponding uptakes of pristine MIL-101(Cr). For instance, [MPPyr][DCA]/MIL-101(Cr) showed lower CH_4 and CO_2 uptakes of 0.02 and 0.91 cm^3/g, respectively, as compared to pristine MIL-101(Cr), 0.28 and 1.59 cm^3/g at 0.1 bar. These decreases in the gas adsorption uptakes were ascribed to the incorporation of IL in the pores of MIL-101 (Cr) resulting in reduced surface area and pore volume of the [MPPyr] [DCA]/MIL-101(Cr) composite. Moreover, the N_2 uptakes in the IL/MOF composite at a low-pressure of 0.1 bar were slightly higher than the detection limit of the equipment. The COSMO-RS calculations performed at 25 °C in a pressure range of 0.1 to 1 bar (**Fig. S6**) demonstrated that N_2 solubility in the [MPPyr][DCA] is almost negligible at low pressures as compared to the significantly high CO_2 solubility, therefore, at low pressures the N_2 uptakes of the [MPPyr][DCA]/MIL-101(Cr) composite are critically low.

Based on the gas adsorption isotherms, ideal CO_2/N_2, CO_2/CH_4, and CH_4/N_2 selectivities of pristine MIL-101(Cr) and [MPPyr][DCA]/MIL-101(Cr) composite were determined up to 1 bar, as shown in Fig. 7**b and c**, respectively. Adsorption selectivity data illustrated that separation performance of [MPPyr][DCA]/MIL-101(Cr) composite was significantly higher than the pristine MIL-101(Cr), especially at low-pressure region. Upon the incorporation of IL, ideal CO_2/N_2 and CH_4/N_2 selectivity of MIL-101(Cr) increased from 17.9 to 64173.1 and from 3.1 to 1874.1, respectively, at 0.1 bar, 25 °C, which corresponds to approximately 3600- and 600-times selectivity improvement for the MOF upon the IL incorporation. In the case of CO_2/CH_4, on the other hand, IL/MOF composite showed six-times improvement with the corresponding selectivity of 34.2 at 0.1 bar. Moreover, the data further demonstrate that [MPPyr][DCA]/MIL-101(Cr) composite offers practically infinite selectivity for CO_2/N_2 and CH_4/N_2 at 0.001 bar as shown in Fig. 7**c**. Comparison of these adsorption selectivity results with other IL/MOF composites reported in the literature is given in **Table S3**, which shows that the [MPPyr][DCA]/MIL-101(Cr) composite offers exceptionally high adsorption selectivities for CO_2/N_2, CO_2/CH_4, and CH_4/N_2, especially at low pressures, outperforming other reported IL/MOF composites.

Furthermore, decreases in CO_2/N_2, CO_2/CH_4, and CH_4/N_2 selectivities of [MPPyr][DCA]/MIL-101(Cr) were observed with an increase in pressure. For instance, at 1 bar, CO_2/N_2, CO_2/CH_4, and CH_4/N_2 selectivities of [MPPyr][DCA]/MIL-101(Cr) composite were measured as 9.4, 28.3, and 3.3, respectively. The decrease in gas uptakes with increasing pressure is attributed to the fact that, at high pressures, gas adsorption is dependent on the available pore volume of the material. However, in the case of low-pressure region, interactions between the adsorbent and the gas molecules become the dominant factor [58]. Therefore, as the adsorption mechanism is changed from surface affinity to pore availability at high pressure, CO_2/N_2, CO_2/CH_4, and CH_4/N_2 selectivities of [MPPyr][DCA]/MIL-101(Cr) composite decreases. Overall, [MPPyr] [DCA]/MIL-101(Cr) composite is highly CO_2 selective in adsorption-based separations especially at low pressures (as demonstrated in **Table S3**), thus it offers a broad potential as a filler to boost the separation performance of a polymer membrane.

3.2.2. Membrane-based separation with MOF/polymer and IL/MOF/polymer MMMs

Permeability measurements of CO_2, N_2, and CH_4 were carried out at 1 bar and 35 °C, and the corresponding CO_2/N_2 and CO_2/CH_4 ideal selectivities were determined for MIL-101(Cr)/Pebax MMMs and [MPPyr][DCA]/MIL-101(Cr)/Pebax MMMs. Fig. 8**a, b, and c** showed CO_2 permeabilities, CO_2/N_2 and CO_2/CH_4 permeation selectivities, respectively, of the MMMs having different loadings of MIL-101(Cr) and [MPPyr][DCA]/MIL-101(Cr) composite. Moreover, the CO_2, N_2, and CH_4 permeability data, along with the CO_2/N_2 and CO_2/CH_4 selectivity

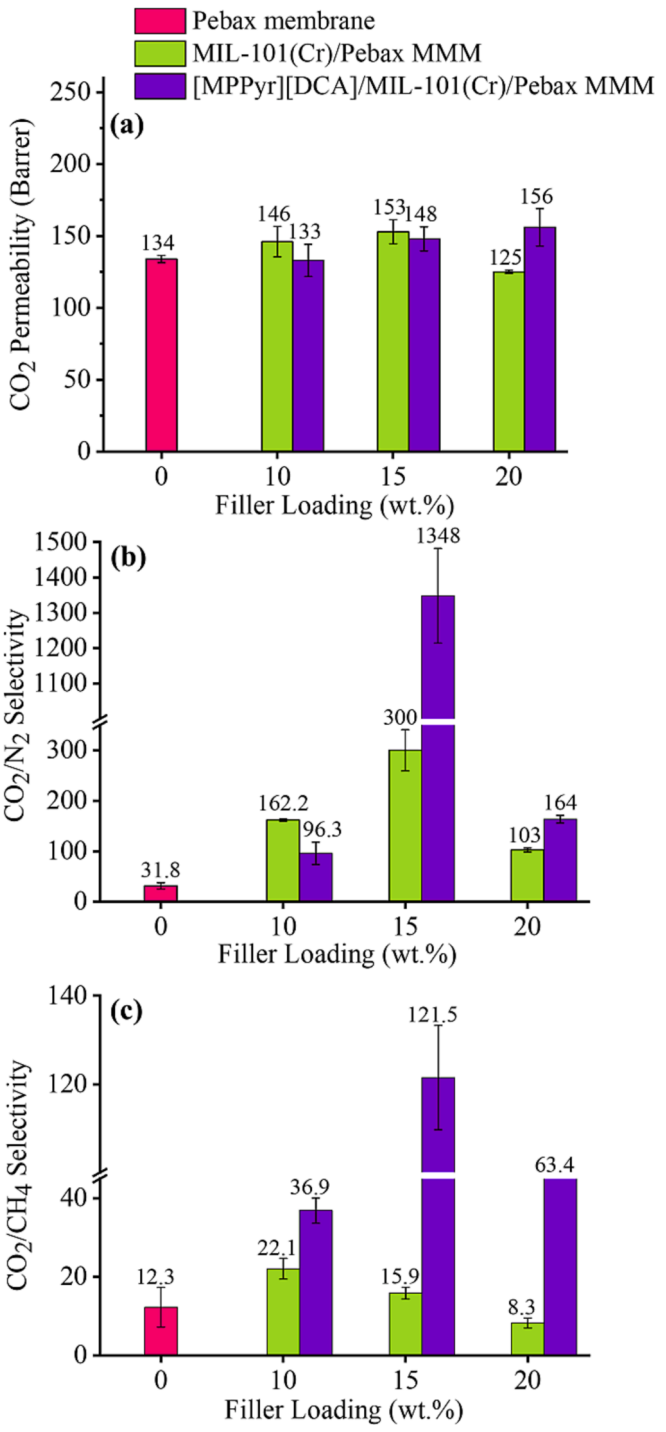


Fig. 8. (a) CO_2 permeability, (b) CO_2/N_2 selectivity, (c) CO_2/CH_4 selectivity of MIL-101(Cr)/Pebax MMMs and [MPPyr][DCA]/MIL-101(Cr)/Pebax MMMs with 10, 15, and 20 wt.% MIL-101(Cr) and [MPPyr][DCA]/MIL-101(Cr) loadings, measured at 1 bar and 35 °C.

data are also given in **Table S4**. Pure Pebax membrane has CO_2, N_2, and CH_4 permeabilities of 134.6 ± 2.1, 4.2 ± 0.5, and 10.9 ± 1.3 Barrer, respectively, with CO_2/N_2 and CO_2/CH_4 selectivities of 31.8 ± 1.7 and 12.3 ± 1.4, respectively. For MIL-101(Cr)/Pebax MMM having 10 wt.% MIL-101(Cr) loading, CO_2, N_2, and CH_4 permeabilities were measured as 146.0 ± 1.1, 0.9 ± 0.8, and 6.6 ± 1.3 Barrer, respectively. The corresponding CO_2/N_2 and CO_2/CH_4 selectivities were calculated as 162.2 ± 20.7 and 22.1 ± 4.6, respectively. As the loading of MIL-101(Cr) in MMM was increased to 15 wt.%, CO_2 and CH_4 permeabilities slightly

increased to 153.0 ± 8.4 and 9.6 ± 0.1 Barrer, respectively, with a further decrease in N_2 permeability to 0.5 ± 0.02 Barrer, leading to CO_2/N_2 and CO_2/CH_4 selectivities of 300.0 ± 40.5 and 15.9 ± 0.9, respectively. These results demonstrated that MIL-101(Cr) filler increased the CO_2 permeability of pure polymer, however, N_2 permeability was significantly decreased, resulting in enhanced CO_2/N_2 selectivity. Overall, MIL-101(Cr)/Pebax MMMs with 10 wt.% filler loading exhibited 5.4-times (1.7-times) improvement in CO_2/N_2 (CO_2/CH_4) selectivity, and the MOF/polymer MMM with 15 wt.% loading showed 10-times (1.2-times) improvement in CO_2/N_2 (CO_2/CH_4) selectivity as compared to pure Pebax. Such improvement in CO_2/N_2 and CO_2/CH_4 selectivities of the MIL-101(Cr)/Pebax MMM can be attributed to the presence of unsaturated Cr(III) sites in MIL-101(Cr) structure offering strong affinity towards CO_2 [38,39].

The CO_2 permeabilities and CO_2/CH_4 selectivities of MIL-101(Cr)/Pebax MMMs obtained in this study are comparable to literature, however, CO_2/N_2 selectivities of MIL-101(Cr)/Pebax MMMs were found to be superior compared to the other MOF/Pebax MMMs reported in the literature. For example, ZIF-8/Pebax MMM having 15 wt.% ZIF-8 loading was reported to have a CO_2 permeability of 100 Barrer at 23 °C and 1 bar [59]. MIL-101(Cr)/Pebax MMM presented in this work has an approximately 1.5-times higher permeability (153 Barrer) than ZIF-8/Pebax MMM. The CO_2/N_2 selectivity of MIL-101(Cr)/Pebax MMM was 8.5-times higher (71) than the reported CO_2/N_2 selectivity (35) of ZIF-8/Pebax MMM with no significant difference in CO_2/CH_4 selectivities. CO_2 permeability and CO_2/CH_4 selectivity of MIL-101(Cr)/Pebax MMM having 15 wt.% MIL-101(Cr) loading was almost the same as BIT-72/Pebax MMM reported in literature at 25 °C and 10 bar [60], however, CO_2/N_2 selectivity was observed to be 5.3-times higher, compared to the highest reported CO_2/N_2 selectivity (56) of BIT-72/Pebax MMM. A more detailed comparison of the synthesized MIL-101(Cr)/Pebax MMMs with the previously reported literature is given in **Table S5** which shows the superior CO_2/N_2 selectivity of MIL-101(Cr)/Pebax MMMs having 10 and 15 wt.% MIL-101(Cr) loadings.

In the case of IL/MOF/polymer MMMs, the separation performance of Pebax membrane was further enhanced with the incorporation of IL/MOF composite. At 10 wt.% [MPPyr][DCA]/MIL-101(Cr) loading, CO_2, N_2, and CH_4 permeabilities were measured as 133.0 ± 11.2, 1.38 ± 0.2, and 3.6 ± 0.3 Barrer, respectively. Based on these results, the corresponding CO_2/N_2 and CO_2/CH_4 selectivities were calculated as 96.3 ± 21.8 and 36.9 ± 3.2, respectively. As the loading of [MPPyr][DCA]/MIL-101(Cr) composite in the MMM was increased to 15 wt.%, CO_2 permeability slightly increased to 148.2 ± 8.4, with a further decrease in CH_4 and N_2 permeabilities to 1.2 ± 0.08 and 0.1 ± 0.02 Barrer, respectively, leading to CO_2/N_2 and CO_2/CH_4 selectivities of 1347 ± 134 and 121.5 ± 11.8, respectively. Incorporation of IL/MOF composite into the polymer slightly changed the CO_2 permeability, however, CH_4 and N_2 exhibited poor permeabilities, resulting in a significant boost in the CO_2/CH_4 and CO_2/N_2 selectivities. Overall, [MPPyr][DCA]/MIL-101(Cr)/Pebax MMMs with 10 wt.% [MPPyr][DCA]/MIL-101(Cr) composite loading exhibited 3.2-times (3-times) improvement in CO_2/N_2 (CO_2/CH_4) selectivity, and with 15 wt.%, the corresponding CO_2/N_2 (CO_2/CH_4) selectivity showed 42-times (9.8-times) improvement compared to the pure Pebax. Moreover, the [MPPyr][DCA]/MIL-101(Cr)/Pebax MMMs having 15 wt.% IL/MOF loading also showed 4.4-times (7.6-times) higher CO_2/N_2 (CO_2/CH_4) selectivity compared to the MIL-101(Cr)/Pebax MMM having 15 wt.% MIL-101(Cr) loading. The ideal CH_4/N_2 selectivities were also computed for pure Pebax, MIL-101(Cr)/Pebax MMMs, and [MPPyr][DCA]/MIL-101(Cr)/Pebax MM as 2.42 ± 1, 6.79 ± 1.1, and 11.9 ± 2.

To compare the separation performance of the best performing IL/MOF/polymer MMM, an IL/polymer MMM and an MMM with free-IL and free-MOF at an identical filler loading (15 wt.%) were synthesized and tested for CO_2/N_2 and CO_2/CH_4 separation (**Table S4**). In the case of IL/polymer MMM, CO_2, N_2, and CH_4 permeabilities were measured as 146.1 ± 7.3, 1.7 ± 0.4, and 2.1 ± 0.4 Barrer, respectively, with the corresponding CO_2/N_2 and CO_2/CH_4 selectivities of 85.9 ± 23.4 and 69.5 ± 15.8, respectively. On the other hand, for free-IL/free-MOF/polymer MMM, the CO_2, N_2, and CH_4 permeabilities were measured as 129.4 ± 8.1, 0.4 ± 0.2, and 2.08 ± 0.5 Barrer, respectively. The corresponding CO_2/N_2 and CO_2/CH_4 selectivities were calculated as 322.5 ± 69.7 and 62.2 ± 10.9, respectively. The IL/MOF/polymer MMM having 15 wt.% IL/MOF composite as a filler showed 4.1- and 1.9-times higher CO_2/N_2 and CO_2/CH_4 selectivity, respectively, as compared to the MMM, which have free-IL and free-MOF as filler.

The exceptionally high gas separation performance of [MPPyr][DCA]/MIL-101(Cr)/Pebax MMMs that we present here can be attributed to the superior solubility of CO_2 in the [MPPyr][DCA], and interactions between IL and CO_2 molecules over N_2 and CH_4. Moreover, IL incorporation into MIL-101(Cr) resulted in reduced pore size of IL/MOF composite compared to pristine MOF, leading to improved molecular sieving effect [29]. Permeability is the physical property of the polymer therefore, CO_2 permeability of all MMMs is not increased. Moreover, it was also observed that by the addition of the filler to the polymer matrix, the d-spacing of the membranes does not change significantly, as a result gas permeabilities were only slightly improved [61,62]. In contrast, the dramatic increases in the CO_2/N_2 selectivities of MMMs compared to pure polymer were attributed to the very poor solubility of N_2 in the bulk [MPPyr][DCA], which was supported by the COSMO-RS calculations. The gas adsorption experiments performed for MIL-101(Cr)/[MPPyr][DCA] composite presented in Fig. 7 also demonstrated significantly low N_2 uptakes. Therefore, low N_2 permeability of the MIL-101(Cr)/[MPPyr][DCA]/Pebax MMM resulted in high CO_2/N_2 selectivity. As discussed in the characterization section, the addition of [MPPyr][DCA] boosted the IL/polymer and IL/MOF interfacial interactions, which resulted in improved gas separation performance of MMMs. Moreover, a decrease in the separation performance of the MMMs was observed when the filler loading was increased beyond 15 wt.%, which was also observed in previous studies [26,63,64]. This change can be attributed to the reduced compatibility between the filler and the polymer at higher loadings and agglomeration of the filler particles [15,65].

CO_2 permeabilities of the MMMs along with their CO_2/N_2 and CO_2/CH_4 selectivities were compared with the Robeson's upper bound as shown in Fig. 9**a and b**, respectively. The gas separation performances of MIL-101(Cr)/Pebax MMMs and [MPPyr][DCA]/MIL-101(Cr)/Pebax MMMs were shown together with the literature data of MOF/polymer MMMs and IL/MOF/polymer MMMs collected under different conditions of temperature and pressure as given in **Table S5**. MIL-101(Cr)/Pebax MMMs and [MPPyr][DCA]/MIL-101(Cr)/Pebax MMMs outperformed the Robeson's upper bound (2008) and previously reported membranes for CO_2/N_2 separation at all loadings. Similarly, in the case of CO_2/CH_4 upper bound (Fig. 9**b**), [MPPyr][DCA]/MIL-101(Cr)/Pebax MMMs having 15 and 20 wt.% [MPPyr][DCA]/MIL-101(Cr) provide superior CO_2/CH_4 selectivity and acceptable CO_2 permeability leading them to surpass the upper bound limit.

Next, we compared the separation performance of [MPPyr][DCA]/MIL-101(Cr)/Pebax MMM with IL/MOF/Pebax MMMs which were reported in the literature and presented in Fig. 9. For example, [BMIM][TF_2N]/ZIF-8/Pebax MMM having 15 wt.% ZIF-8 loading was reported to have CO_2 permeability of 105 Barrer and CO_2/N_2 selectivity of 84.5 at 1 bar and 25 °C [29]. The [MPPyr][DCA]/MIL-101(Cr)/Pebax having 15 wt.% [MPPyr][DCA]/MIL-101(Cr) synthesized in this work showed 1.4- and 16-times improved CO_2 permeability (148 Barrer) and CO_2/N_2 selectivity (1347), respectively, than the [BMIM][Tf_2N]/ZIF/Pebax MMM with no significant difference in CO_2/CH_4 selectivities.

[MPPyr][DCA]/MIL-101(Cr)/Pebax MMM having 15 wt.% of filler loading was also compared with the [BMIM][PF_6]/ZIF-8/Pebax MMMs reported at 3 bar and 35 °C [66]. It was observed that the CO_2 permeability and CO_2/N_2 selectivity of [MPPyr][DCA]/MIL-101(Cr)/Pebax MMM were 1.2- and 15.8-times higher compared to the best performing [BMIM][PF_6]/ZIF-8/Pebax having CO_2 permeability of 120 Barrer and CO_2/N_2 selectivity of 85. **Table S4** showed that CO_2/N_2 selectivities

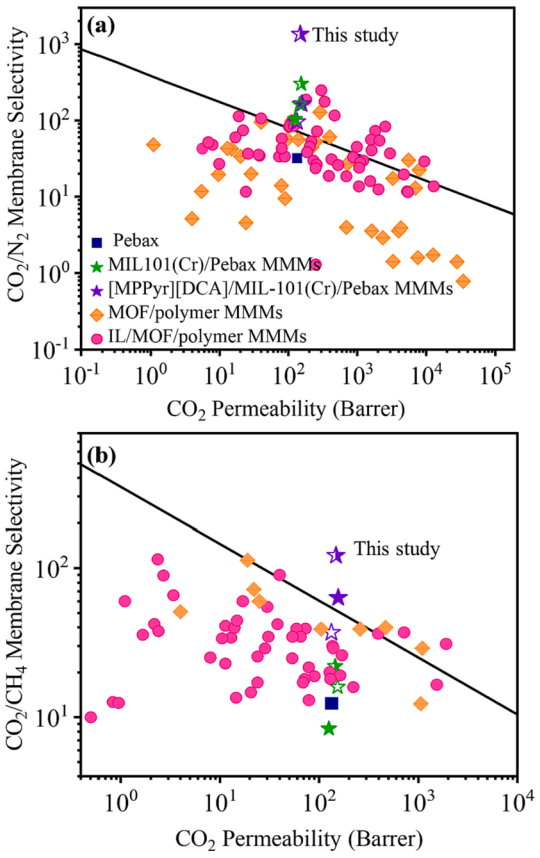


Fig. 9. (a) Comparison of CO_2/N_2 selectivity, (b) CO_2/CH_4 selectivity and CO_2 permeability of MMMs synthesized in this study with the literature data. The line represents the Robeson's upper bound [3]. The open star represents 10 wt. % filler loading, half closed, and fully closed stars represent 15 wt.% and 20 wt. % filler loading, respectively. Details of the data shown in this figure are reported in **Table S5**.

of [MPPyr][DCA]/MIL101(Cr)/Pebax MMMs presented in this study, especially with 15 wt.% [MPPyr][DCA]/MIL101(Cr) loading, are superior to all the literature data reported up to date. In view of these comparisons, the selectivity data reported here set a new benchmark for CO_2/N_2 separation, demonstrating a broad potential of incorporating pyrrolidinium-based IL/MOF composites in polymers to fabricate IL/MOF/polymer MMMs. The results will significantly contribute to the literature of MMMs for accelerating the design and development of new IL/MOF/polymer MMMs in near future.

The reproducibility of the separation results was confirmed by synthesizing the MMMs several times to obtain different batches of the same membrane, which were then tested under identical conditions, and the separation performances of each batch were compared with each other. Moreover, for the long-term stability tests of [MPPyr][DCA]/MIL-101(Cr)/Pebax MMM given in Fig. 10, we synthesized the MMM from scratch, and it was observed that the results are in the error range of what we reported in the gas permeation results with a different batch of the MMM. The long-term gas separation performance of the [MPPyr][DCA]/MIL-101(Cr)/Pebax MMM with 15 wt.% [MPPyr][DCA]/MIL-101(Cr) loading was also investigated up to 75 h to evaluate the stability of the membrane under continuous operating conditions. Data presented in Fig. 10 showed that the data fluctuated within a narrow range having CO_2 permeability of 151 ± 5.9 Barrer with corresponding average CO_2/N_2 and CO_2/CH_4 selectivities of 1298 ± 208 and 116 ± 9.7, respectively. The results showed a good long-term working stability of IL/MOF/polymer MMM synthesized in this work, making it a promising gas separation material.

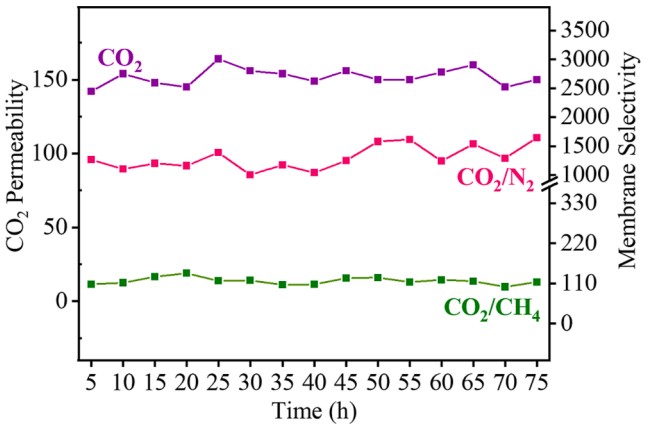


Fig. 10. Long-term stability test of [MPPyr][DCA]/MIL-101(Cr)/Pebax MMM with 15 wt.% [MPPyr][DCA]/MIL-101(Cr) loading.

4. Conclusion

We combined the highly CO_2-selective MIL-101(Cr) and a pyrrolidinium-based IL, [MPPyr][DCA], to prepare a novel IL/MOF composite which showed excellent CO_2/N_2, CO_2/CH_4 and CH_4/N_2 adsorption selectivities. The [MPPyr][DCA]/MIL-101(Cr) composite was incorporated into Pebax to generate [MPPyr][DCA]/MIL-101(Cr)/Pebax MMMs which showed exceptional CO_2/N_2 and CO_2/CH_4 separation performances. At 15 wt.% [MPPyr][DCA]/MIL-101(Cr) loading, the MMM showed an improved CO_2 permeability of 148 Barrer with significantly higher CO_2/N_2 (1347) and CO_2/CH_4 (121.5) selectivity as compared to the pure Pebax having a CO_2 permeability of 134 Barrer with CO_2/N_2 and CO_2/CH_4 selectivities of 31.8 and 12.3, respectively. The CO_2/N_2 and CO_2/CH_4 selectivities of [MPPyr][DCA]/MIL-101(Cr)/Pebax MMM having 15 wt.% [MPPyr][DCA]/MIL-101(Cr) loading was observed to be 42- and 9.8-times higher than the pure Pebax membrane, respectively, and significantly superior to all other IL/MOF/polymer MMMs reported in the literature. All the [MPPyr][DCA]/MIL-101(Cr)/Pebax MMMs that we synthesized in this work were located above the Robeson's upper bound for CO_2/N_2 separation. Results showed the outstanding performance of [MPPyr][DCA]/MIL-101(Cr)/Pebax MMMs, especially for CO_2/N_2 separation. Considering the existence of a large number and variety of ILs, MOFs, and polymers, our results will contribute significantly into the development of new IL/MOF/polymer MMMs for various gas separations by setting a new benchmark for CO_2/N_2 selectivity.

CRediT authorship contribution statement

Nitasha Habib: Methodology, Investigation, Writing – original draft, Writing – review & editing. **Özce Durak:** Methodology, Investigation, Writing – original draft, Writing – review & editing. **Alper Uzun:** Conceptualization, Supervision, Methodology, Writing – original draft, Writing – review & editing. **Seda Keskin:** Conceptualization, Supervision, Methodology, Writing – original draft, Writing – review & editing.

Declaration of Competing Interest

The authors declare that they have no known competing financial interests or personal relationships that could have appeared to influence the work reported in this paper.

Data availability

Data will be made available on request.

Acknowledgements

The authors gratefully acknowledge the support of Koc University TUPRAŞ Energy Center (KUTEM) and Koc University Surface Science and Technology Center (KUYTAM). S.K. acknowledges ERC-2017-Starting Grant. This study was funded by the European Research Council under the European Union's Horizon 2020 research and innovation programme (ERC-2017-Starting Grant, grant agreement no. 756489-COSMOS).

Appendix A. Supplementary data

Supplementary data to this article can be found online at https://doi.org/10.1016/j.seppur.2023.123346.

References

[1] Y. Yampolskii, Polymeric gas separation membranes, Macromolecules 45 (8) (2012) 3298–3311, https://doi.org/10.1021/ma300213b.
[2] E. Favre, Membrane processes and postcombustion carbon dioxide capture: Challenges and prospects, Chem. Eng. J. 171 (3) (2011) 782–793, https://doi.org/10.1016/j.cej.2011.01.010.
[3] L.M. Robeson, The upper bound revisited, J. Membr. Sci. 320 (1–2) (2008) 390–400.
[4] J. Dechnik, J. Gascon, C.J. Doonan, C. Janiak, C.J. Sumby, Mixed-matrix membranes, Angew. Chem. Int. Ed. 56 (32) (2017) 9292–9310, https://doi.org/10.1002/anie.201701109.
[5] M.M. Zagho, M.K. Hassan, M. Khraisheh, M.A.A. Al-Maadeed, S. Nazarenko, A review on recent advances in CO_2 separation using zeolite and zeolite-like materials as adsorbents and fillers in mixed matrix membranes (MMMs), Chem. Eng. J. Adv. 6 (2021) 100091, https://doi.org/10.1016/j.ceja.2021.100091.
[6] M. Rezakazemi, A.E. Amooghin, M.M. Montazer-Rahmati, A.F. Ismail, T. Matsuura, State-of-the-art membrane based CO_2 separation using mixed matrix membranes (MMMs): An overview on current status and future directions, Prog. Polym. Sci. 39 (5) (2014) 817–861, https://doi.org/10.1016/j.progpolymsci.2014.01.003.
[7] A.L. Khan, N. Habib, M. Aslam, Metal organic frameworks-based mixed matrix membranes for gas separation, Elsevier, Nanomaterials for Air Remediation, 2020, pp. 273–292.
[8] Y. Wang, G. Yang, H. Guo, X. Meng, G. Kong, Z. Kang, R. Guillet-Nicolas, S. Mintova, Preparation of HKUST-1/PEI mixed-matrix membranes: adsorption-diffusion coupling control of small gas molecules, J. Membr. Sci. 643 (2022) 120070, https://doi.org/10.1016/j.memsci.2021.120070.
[9] R. Thür, N. Van Velthoven, S. Slootmaekers, J. Didden, R. Verbeke, S. Smolders, M. Dickmann, W. Egger, D. De Vos, I.F. Vankelecom, Bipyridine-based UiO-67 as novel filler in mixed-matrix membranes for CO_2-selective gas separation, J. Membr. Sci. 576 (2019) 78–87, https://doi.org/10.1016/j.memsci.2019.01.016.
[10] N. Habib, Z. Shamair, N. Tara, A.-S. Nizami, F.H. Akhtar, N.M. Ahmad, M.A. Gilani, M.R. Bilad, A.L. Khan, Development of highly permeable and selective mixed matrix membranes based on Pebax® 1657 and NOTT-300 for CO_2 capture, Sep. Purif. Technol. 234 (2020) 116101.
[11] Q. Zhao, S. Lian, R. Li, Z. Yu, Q. Liu, G.-L. Zang, C. Song, Architecting MOFs-Based Mixed Matrix Membrane for Efficient CO_2 Separation: Ameliorating Strategies Toward Non-Ideal Interface, Chem. Eng. J. (2022), 136290, https://doi.org/10.1016/j.cej.2022.136290.
[12] M. Gou, R. Guo, H. Cao, W. Zhu, F. Liu, Z. Wei, An MOF-tailored hierarchical porous microenvironment for CO_2 as an efficient filler for mixed matrix membranes, Chem. Eng. J. 438 (2022) 135651, https://doi.org/10.1016/j.cej.2022.135651.
[13] M.S. Buddin, A. Ahmad, A review on metal-organic frameworks as filler in mixed matrix membrane: Recent strategies to surpass upper bound for CO_2 separation, J. CO_2 Utiliz. 51 (2021) 101616, https://doi.org/10.1016/j.jcou.2021.101616.
[14] W. Chen, Z. Zhang, L. Hou, C. Yang, H. Shen, K. Yang, Z. Wang, Metal-organic framework MOF-801/PIM-1 mixed-matrix membranes for enhanced CO_2/N_2 separation performance, Sep. Purif. Technol. 250 (2020) 117198, https://doi.org/10.1016/j.seppur.2020.117198.
[15] M.J.C. Ordonez, K.J. Balkus Jr, J.P. Ferraris, I.H. Musselman, Molecular sieving realized with ZIF-8/Matrimid® mixed-matrix membranes, J. Membr. Sci. 361 (1–2) (2010) 28–37.
[16] X. Guo, Z. Qiao, D. Liu, C. Zhong, Mixed-matrix membranes for CO_2 separation: Role of the third component, J. Mater. Chem. A 7 (43) (2019) 24738–24759, https://doi.org/10.1039/C9TA09012F.
[17] S. Cong, Q. Shen, M. Shan, J. Wang, J. Liu, Y. Zhang, Enhanced permeability in mixed matrix membranes for CO_2 capture through the structural regulation of the amino-functionalized Co/ZIF-8 heterometallic nanoparticles, Chem. Eng. J. 383 (2020) 123137, https://doi.org/10.1016/j.cej.2019.123137.
[18] W. Jiang, X. Li, G. Gao, F. Wu, C. Luo, L. Zhang, Advances in applications of ionic liquids for phase change CO_2 capture, Chem. Eng. J. (2022) 136767, https://doi.org/10.1016/j.cej.2022.136767.
[19] Ö. Durak, M. Zeeshan, N. Habib, H.C. Gülbalkan, A.A.A.M. Alsuhile, H.P. Çağlayan, S.F. Kurtoğlu-Öztulum, Y. Zhao, Z.P. Haslak, A. Uzun, Composites of porous materials with ionic liquids: Synthesis, characterization, applications, and beyond, Micropor. Mesopor. Mater. (2022) 111703, https://doi.org/10.1016/j.micromeso.2022.111703.
[20] M. Zeeshan, V. Nozari, M.B. Yagci, T. Isık, U. Unal, V. Ortalan, S. Keskin, A. Uzun, Core–shell type ionic liquid/metal organic framework composite: an exceptionally high CO_2/CH_4 selectivity, J. Am. Chem. Soc. 140 (32) (2018) 10113–10116, https://doi.org/10.1021/jacs.8b05802.
[21] M. Zeeshan, S. Keskin, A. Uzun, Enhancing CO_2/CH_4 and CO_2/N_2 separation performances of ZIF-8 by post-synthesis modification with [BMIM][SCN], Polyhedron 155 (2018) 485–492.
[22] H.M. Polat, M. Zeeshan, A. Uzun, S. Keskin, Unlocking CO_2 separation performance of ionic liquid/CuBTC composites: Combining experiments with molecular simulations, Chem. Eng. J. 373 (2019) 1179–1189, https://doi.org/10.1016/j.cej.2019.05.113.
[23] M. Zeeshan, H. Kulak, S. Kavak, H.M. Polat, O. Durak, S. Keskin, A. Uzun, Influence of anion size and electronic structure on the gas separation performance of ionic liquid/ZIF-8 composites, Micropor. Mesopor. Mater. 306 (2020) 110446.
[24] I.C. Ferreira, T.J. Ferreira, A.D. Barbosa, B. de Castro, R.P. Ribeiro, J.P. Mota, V. D. Alves, L. Cunha-Silva, I.A. Esteves, L.A. Neves, Cr-based MOF/IL composites as fillers in mixed matrix membranes for CO_2 separation, Sep. Purif. Technol. 276 (2021) 119303.
[25] I. Yasmeen, A. Ilyas, Z. Shamair, M.A. Gilani, S. Rafiq, M.R. Bilad, A.L. Khan, Synergistic effects of highly selective ionic liquid confined in nanocages: Exploiting the three component mixed matrix membranes for CO_2 capture, Chem. Eng. Res. Des. 155 (2020) 123–132.
[26] N. Habib, O. Durak, M. Zeeshan, A. Uzun, S. Keskin, A novel IL/MOF/polymer mixed matrix membrane having superior CO_2/N_2 selectivity, J. Membr. Sci. 658 (2022) 120712, https://doi.org/10.1016/j.memsci.2022.120712.
[27] Z. Iqbal, Z. Shamair, M. Usman, M.A. Gilani, M. Yasin, S. Saqib, A.L. Khan, One pot synthesis of UiO-66@IL composite for fabrication of CO_2 selective mixed matrix membranes, Chemosphere (2022) 135122, https://doi.org/10.1016/j.chemosphere.2022.135122.
[28] J. Ma, Y. Ying, X. Guo, H. Huang, D. Liu, C. Zhong, Fabrication of mixed-matrix membrane containing metal–organic framework composite with task-specific ionic liquid for efficient CO_2 separation, J. Mater. Chem. A 4 (19) (2016) 7281–7288, https://doi.org/10.1039/C6TA02611G.
[29] H. Li, L. Tuo, K. Yang, H.-K. Jeong, Y. Dai, G. He, W. Zhao, Simultaneous enhancement of mechanical properties and CO_2 selectivity of ZIF-8 mixed matrix membranes: Interfacial toughening effect of ionic liquid, J. Membr. Sci. 511 (2016) 130–142.
[30] Z. Guo, W. Zheng, X. Yan, Y. Dai, X. Ruan, X. Yang, X. Li, N. Zhang, G. He, Ionic Liquid Tuning Nanocage Size of MOFs through a two-step adsorption/infiltration strategy for Enhanced Gas Screening of Mixed-matrix membranes, J. Membr. Sci. 118101 (2020).
[31] Z. Zhang, X. Cao, C. Geng, Y. Sun, Y. He, Z. Qiao, C. Zhong, Machine learning aided high-throughput prediction of ionic liquid@MOF composites for membrane-based CO_2 capture, J. Membr. Sci. 650 (2022) 120399, https://doi.org/10.1016/j.memsci.2022.120399.
[32] H. Rajati, A.H. Navarchian, D. Rodrigue, S. Tangestaninejad, Effect of immobilizing ionic liquid on amine-functionalized MIL-101 (Cr) incorporated in Matrimid membranes for CO_2/CH_4 separation, Chem. Eng. Process. Process Intensif. 168 (2021) 108590, https://doi.org/10.1016/j.cep.2021.108590.
[33] Y. Zhang, H. Jia, Q. Wang, W. Ma, G. Yang, S. Xu, S. Li, G. Su, Y. Qu, M. Zhang, Optimization of a MOF Blended with Modified Polyimide Membrane for High-Performance Gas Separation, Membranes 12 (1) (2021) 34, https://doi.org/10.3390/membranes12010034.
[34] J. Gorman, Faster, better, cleaner?: New liquids take aim at old-fashioned chemistry, Sci. News 160 (10) (2001) 156–158, https://doi.org/10.2307/4012654.
[35] The Cambridge Structural Databse (CSD). https://www.ccdc.cam.ac.uk/CCDCStats/Stats, (accessed December 2, 2022.
[36] M. Zeeshan, H.C. Gulbalkan, O. Durak, Z.P. Haslak, U. Unal, S. Keskin, A. Uzun, An Integrated Computational-Experimental Hierarchical Approach for the Rational Design of an IL/UiO-66 Composite Offering Infinite CO_2 Selectivity, Adv. Funct. Mater. (2022) 2204149, https://doi.org/10.1002/adfm.202204149.
[37] A. Mahapatra, M. Chakraborty, S. Barik, M. Sarkar, Comparison between pyrrolidinium-based and imidazolium-based dicationic ionic liquids: intermolecular interaction, structural organization, and solute dynamics, PCCP 23 (37) (2021) 21029–21041, https://doi.org/10.1039/D1CP02790E.
[38] P.L. Llewellyn, S. Bourrelly, C. Serre, A. Vimont, M. Daturi, L. Hamon, G. De Weireld, J.-S. Chang, D.-Y. Hong, Y. Kyu Hwang, High uptakes of CO_2 and CH_4 in mesoporous metal organic frameworks MIL-100 and MIL-101, Langmuir 24 (14) (2008) 7245–7250, https://doi.org/10.1021/la800227x.
[39] P. Chowdhury, C. Bikkina, S. Gumma, Gas adsorption properties of the chromium-based metal organic framework MIL-101, J. Phys. Chem. C 113 (16) (2009) 6616–6621, https://doi.org/10.1021/jp811418r.
[40] A. Akçay, V. Balci, A. Uzun, Structural factors controlling thermal stability of imidazolium ionic liquids with 1-*n*-butyl-3-methylimidazolium cation on γ-Al_2O_3, Thermochim Acta 589 (2014) 131–136, https://doi.org/10.1016/j.tca.2014.05.018.
[41] M. Wojdyr, Fityk: a general-purpose peak fitting program, J. Appl. Cryst. 43 (5 Part 1) (2010) 1126–1128, https://doi.org/10.1107/S0021889810030499.
[42] S. Lee, J.H. Lee, J. Kim, User-friendly graphical user interface software for ideal adsorbed solution theory calculations, Korean J. Chem. Eng. 35 (1) (2018) 214–221, https://doi.org/10.1007/s11814-017-0269-9.
[43] Ö. Durak, H. Kulak, S. Kavak, H.M. Polat, S. Keskin, A. Uzun, Towards complete elucidation of structural factors controlling thermal stability of IL/MOF

composites: effects of ligand functionalization on MOFs, J. Phys. Condens. Matter 32 (48) (2020) 484001, https://doi.org/10.1088/1361-648X/aba06c.
[44] D. Yin, C. Li, H. Ren, O. Shekhah, J. Liu, C. Liang, Efficient Pd@ MIL-101(Cr) hetero-catalysts for 2-butyne-1, 4-diol hydrogenation exhibiting high selectivity, RSC Adv. 7 (3) (2017) 1626–1633, https://doi.org/10.1039/C6RA25722D.
[45] Y. Ban, Z. Li, Y. Li, Y. Peng, H. Jin, W. Jiao, A. Guo, P. Wang, Q. Yang, C. Zhong, Confinement of ionic liquids in nanocages: tailoring the molecular sieving properties of ZIF-8 for membrane-based CO_2 capture, Angew. Chem. Int. Ed. 54 (51) (2015) 15483–15487.
[46] A. Jalal, Y. Zhao, A. Uzun, Pyrolysis Temperature Tunes the Catalytic Properties of CuBTC-Derived Carbon-Embedded Copper Catalysts for Partial Hydrogenation, Ind. Eng. Chem. Res. (2022).
[47] M. Zeeshan, V. Nozari, S. Keskin, A. Uzun, Structural factors determining thermal stability limits of ionic liquid/MOF composites: imidazolium ionic liquids combined with CuBTC and ZIF-8, Ind. Eng. Chem. Res. 58 (31) (2019) 14124–14138.
[48] O. Palumbo, F. Trequattrini, J.-B. Brubach, P. Roy, A. Paolone, Molecular assembling in mixtures of hydrophilic 1-butyl-1-methylpyrrolidinium dicyanamide ionic liquid and water, Appl. Sci. 10 (14) (2020) 4837, https://doi.org/10.3390/app10144837.
[49] F. Zhou, J. Zhou, X. Gao, C. Kong, L. Chen, Facile synthesis of MOFs with uncoordinated carboxyl groups for selective CO_2 capture via postsynthetic covalent modification, RSC Adv. 7 (7) (2017) 3713–3719, https://doi.org/10.1039/C6RA25396B.
[50] Y.-K. Seo, G. Hundal, I.T. Jang, Y.K. Hwang, C.-H. Jun, J.-S. Chang, Microwave synthesis of hybrid inorganic–organic materials including porous $Cu_3(BTC)_2$ from Cu (II)-trimesate mixture, Micropor. Mesopor. Mater. 119 (1–3) (2009) 331–337.
[51] L. Gong, Z. Cai, Q. Wu, L. Liu, C. Wang, L. Shan, X. Meng, S. Luo, Z. Liu, S. Zhang, Ionic liquid enhancement of interface compatibility in mixed-linker ZIF-based mixed matrix membranes for advanced CO_2/CH_4 separation, J. Mater. Chem. A (2022), https://doi.org/10.1039/D2TA05767K.
[52] L. Xiang, Y. Pan, G. Zeng, J. Jiang, J. Chen, C. Wang, Preparation of poly (ether-block-amide)/attapulgite mixed matrix membranes for CO_2/N_2 separation, J. Membr. Sci. 500 (2016) 66–75.
[53] B. Monteiro, A.R. Nabais, F.A. Almeida Paz, L. Cabrita, L.C. Branco, I.M. Marrucho, L.A. Neves, C.C. Pereira, Membranes with a low loading of Metal-Organic Framework-Supported Ionic Liquids for CO_2/N_2 separation in CO_2 capture, Energ. Technol. 5 (12) (2017) 2158–2162, https://doi.org/10.1002/ente.201700228.
[54] R.S. Murali, A. Ismail, M. Rahman, S. Sridhar, Mixed matrix membranes of Pebax-1657 loaded with 4A zeolite for gaseous separations, Sep. Purif. Technol. 129 (2014) 1–8.
[55] A. Ghadimi, M. Amirilargani, T. Mohammadi, N. Kasiri, B. Sadatnia, Preparation of alloyed poly (ether block amide)/poly (ethylene glycol diacrylate) membranes for separation of CO_2/H_2 (syngas application), J. Membr. Sci. 458 (2014) 14–26.
[56] Y. Wang, J. Ren, M. Deng, Ultrathin solid polymer electrolyte PEI/Pebax2533/$AgBF_4$ composite membrane for propylene/propane separation, Sep. Purif. Technol. 77 (1) (2011) 46–52.
[57] N. Sharma, N. Sharma, P. Srinivasan, S. Kumar, J.B.B. Rayappan, K. Kailasam, Heptazine based organic framework as a chemiresistive sensor for ammonia detection at room temperature, J. Mater. Chem. A 6 (38) (2018) 18389–18395, https://doi.org/10.1039/C8TA06937A.
[58] F.P. Kinik, C. Altintas, V. Balci, B. Koyuturk, A. Uzun, S. Keskin, [BMIM][PF_6] incorporation doubles CO_2 selectivity of ZIF-8: elucidation of interactions and their consequences on performance, ACS Appl. Mater. Interfaces 8 (45) (2016) 30992–31005, https://doi.org/10.1021/acsami.6b11087.
[59] M. Li, X. Zhang, S. Zeng, H. Gao, J. Deng, Q. Yang, S. Zhang, Pebax-based composite membranes with high gas transport properties enhanced by ionic liquids for CO_2 separation, RSC Adv. 7 (11) (2017) 6422–6431, https://doi.org/10.1039/C6RA27221E.
[60] N. Tara, Z. Shamair, N. Habib, M. Craven, M.R. Bilad, M. Usman, X. Tu, A.L. Khan, Simultaneous increase in CO_2 permeability and selectivity by BIT-72 and modified BIT-72 based mixed matrix membranes, Chem. Eng. Res. Des. 178 (2022) 136–147.
[61] G. Clarizia, P. Bernardo, A Review of the Recent Progress in the Development of Nanocomposites Based on Poly (ether-block-amide) Copolymers as Membranes for CO_2 Separation, Polymers 14 (1) (2021) 10.
[62] C. Soto, B. Comesaña-Gandara, Á. Marcos, P. Cuadrado, L. Palacio, Á.E. Lozano, C. Álvarez, P. Prádanos, A. Hernandez, Thermally Rearranged Mixed Matrix Membranes from Copoly (o-hydroxyamide) s and Copoly (o-hydroxyamide-amide) s with a Porous Polymer Network as a Filler—A Comparison of Their Gas Separation Performances, Membranes 12 (10) (2022) 998.
[63] M.Z. Ahmad, T.A. Peters, N.M. Konnertz, T. Visser, C. Téllez, J. Coronas, V. Fila, W. M. de Vos, N.E. Benes, High-pressure CO_2/CH_4 separation of Zr-MOFs based mixed matrix membranes, Sep. Purif. Technol. 230 (2020) 115858.
[64] X. Li, Y. Cheng, H. Zhang, S. Wang, Z. Jiang, R. Guo, H. Wu, Efficient CO_2 capture by functionalized graphene oxide nanosheets as fillers to fabricate multi-permselective mixed matrix membranes, ACS Appl. Mater. Interfaces 7 (9) (2015) 5528–5537.
[65] W. Chen, Z. Zhang, C. Yang, J. Liu, H. Shen, K. Yang, Z. Wang, PIM-based mixed-matrix membranes containing MOF-801/ionic liquid nanocomposites for enhanced CO_2 separation performance, J. Membr. Sci. 636 (2021) 119581.
[66] Z. Guo, W. Zheng, X. Yan, Y. Dai, X. Ruan, X. Yang, X. Li, N. Zhang, G. He, Ionic liquid tuning nanocage size of MOFs through a two-step adsorption/infiltration strategy for enhanced gas screening of mixed-matrix membranes, J. Membr. Sci. 605 (2020) 118101, https://doi.org/10.1016/j.memsci.2020.118101.